Geophys. J. Int. (2000) **140,** 442–452

Induction arrows from offshore floating magnetometers using land reference data

A. P. Hitchman,[1] F. E. M. Lilley[1] and P. R. Milligan[2]

[1] *Research School of Earth Sciences, Australian National University, Canberra* ACT 0200, *Australia. E-mail: adrian@rses.anu.edu.au*
[2] *Australian Geological Survey Organisation,* GPO Box 378, *Canberra* ACT 2601, *Australia*

Accepted 1999 September 23. Received 1999 September 3; in original form 1999 June 29

SUMMARY

Induction arrows are a traditional output of magnetovariational experiments, and represent transfer functions used quantitatively in the inversion of geomagnetic depth sounding data to give Earth electrical conductivity structure. In this paper, a technique is tested in which 'total-field' variations are combined with horizontal-field data recorded simultaneously at remote stations in order to derive induction arrows. The method is first demonstrated using total-field data recorded on land by an aeromagnetic base station, and then applied to data obtained from magnetometers floated offshore on the sea surface. The floating magnetometers were deployed in two configurations: one tethered to the seafloor; the second free-floating.

Key words: electrical conductivity, electromagnetic induction, floating magnetometer, geomagnetism, induction arrows, total magnetic field.

1 INTRODUCTION

The use of natural time fluctuations in the geomagnetic field to study Earth electrical conductivity structure is commonly described as the method of geomagnetic depth sounding (GDS), or magnetovariations (Weaver 1994). The natural source fields used are more powerful and of a larger scale than the artificial source fields that can be engineered for controlled-source electromagnetic methods. In its simplest form, the GDS method is based primarily on characteristics of the vertical component of the fluctuating field. This signal is normalized in terms of the horizontal fluctuating field, and analysed as a frequency- and polarization-dependent function of the horizontal fluctuating field (Parkinson & Hutton 1989). The method has traditionally been applied to data observed at land sites (Gough & Ingham 1983; Gough 1989).

Offshore, there is no less interest in determining the conductivity structure of the major tectonic features such as subduction slabs and spreading ridges (Heinson *et al.* 1996; Palshin 1996). Instrumentation developed for such applications has generally involved seafloor deployments, both of recording magnetometers as such, and as full magnetotelluric recording stations that measure the local electric fields in addition to the magnetovariational fields (Filloux 1987).

The present paper introduces a new technique, in which observations from total-field magnetometers are used, combined with horizontal data from a reference site. Total-field magnetometers can be regarded as measuring the component of the fluctuating field resolved in the direction of the steady main field. This latter point is made by Parkinson (1983) and Blakeley (1995) for small changes of the total field with space, and by Lilley (1991) for small changes with time. An adaption of the usual theory then produces transfer functions and induction arrows. Total-field variations have been used with horizontal variations in both the magnetic and geographic reference frames to determine transfer functions.

This new technique is tested using total-field data from three different styles of magnetometer deployment. It is first applied to data from an aeromagnetic base station. Next, data from a magnetometer floating at the sea surface while tethered to the seafloor are used. In this novel mode of deployment, the magnetometer is less stable than the base station, but still relatively stationary. Finally, the technique is tested on data from a magnetometer floating at the sea surface and free to drift with ocean currents.

In the examples in the present paper, the geographic position of the magnetometer is determined by satellite navigation. The ARGOS Satellite Information Technology system is used, with oceanic drifter buoys (model SC40) connected to the floating magnetometer package. In the design and deployment of the floating apparatus, care is taken to minimize magnetic components and to ensure that the magnetometer sensor remains sufficiently remote from those items containing unavoidable magnetic material that stray magnetic fields do not contaminate the recorded time-series.

1.1 Notation and Fourier transform convention

Table 1 lists the notation adopted in this paper for time-series representing the different components of magnetic field variation; notation for the corresponding Fourier transforms in the frequency domain is also given. The form adopted for the

Table 1. Notations for the time- and frequency-domain representations of components of magnetic field variation.

Magnetic field direction	Time domain	Frequency domain
Horizontal magnetic north	$h(t)$	$\tilde{h}(\omega)$
Horizontal magnetic east	$d(t)$	$\tilde{d}(\omega)$
Horizontal geographic north	$x(t)$	$\tilde{x}(\omega)$
Horizontal geographic east	$y(t)$	$\tilde{y}(\omega)$
Vertically down	$z(t)$	$\tilde{z}(\omega)$
Total field (amplitude)	$f(t)$	$\tilde{f}(\omega)$

Fourier transform is, giving the case of $h(t)$ as an example,

$$\tilde{h}(\omega) = \int_{-\infty}^{\infty} h(t)\, \mathrm{e}^{-i\omega t}\, dt\,, \tag{1}$$

so that the inverse transform has an implied time dependence of $\mathrm{e}^{+i\omega t}$. In accordance with this time dependence, quadrature induction arrows, after their determination by transfer functions is achieved, are reversed and then plotted (Lilley & Arora 1982). Real arrows are also reversed, as is usual (Hobbs 1992).

Subscripts r and q will be used to denote the real and quadrature parts of a complex quantity.

2 BASIC THEORY

The basic equation for the determination of magnetovariational transfer functions $A(\omega)$ and $B(\omega)$ in the geomagnetic reference frame is

$$\tilde{z}(\omega) = A(\omega)\tilde{h}(\omega) + B(\omega)\tilde{d}(\omega) \tag{2}$$

(Hobbs 1992), where $A(\omega)$ and $B(\omega)$ should be dependent upon local electrical conductivity structure only. If not $z(t)$ but $f(t)$ is known, then as shown by Lilley *et al.* (1984), transfer functions $A_{\mathrm{F}}(\omega)$ and $B_{\mathrm{F}}(\omega)$ for the total field may be determined by finding a best fit of observed data to the equation

$$\tilde{f}(\omega) = A_{\mathrm{F}}(\omega)\tilde{h}(\omega) + B_{\mathrm{F}}(\omega)\tilde{d}(\omega)\,, \tag{3}$$

and $A(\omega)$ and $B(\omega)$ are then determined from

$$A_{\mathrm{r}} = (A_{F_{\mathrm{r}}} - \cos\mathscr{I})/\sin\mathscr{I}\,, \tag{4}$$

$$A_{\mathrm{q}} = A_{F_{\mathrm{q}}}/\sin\mathscr{I}\,, \tag{5}$$

$$B_{\mathrm{r}} = B_{F_{\mathrm{r}}}/\sin\mathscr{I}\,, \tag{6}$$

$$B_{\mathrm{q}} = B_{F_{\mathrm{q}}}/\sin\mathscr{I}\,, \tag{7}$$

where $\mathscr{I}$ is the known (and necessarily non-zero) local inclination of the main geomagnetic field. For Australian stations, $\mathscr{I}$ may be taken from Lewis & McEwin (1996).

If the horizontal variations have been recorded in a geographic reference frame, eq. (2) becomes, for the determination of (geographic frame) transfer functions $P(\omega)$ and $Q(\omega)$,

$$\tilde{z}(\omega) = P(\omega)\tilde{x}(\omega) + Q(\omega)\tilde{y}(\omega)\,. \tag{8}$$

The equivalent of eq. (3) for a geographic reference frame is

$$\tilde{f}(\omega) = P_{\mathrm{F}}(\omega)\tilde{x}(\omega) + Q_{\mathrm{F}}(\omega)\tilde{y}(\omega)\,, \tag{9}$$

with $P(\omega)$ and $Q(\omega)$ determined from

$$P_{\mathrm{r}} = (P_{F_{\mathrm{r}}} - \cos\mathscr{D}\cos\mathscr{I})/\sin\mathscr{I}\,, \tag{10}$$

$$P_{\mathrm{q}} = P_{F_{\mathrm{q}}}/\sin\mathscr{I}\,, \tag{11}$$

$$Q_{\mathrm{r}} = (Q_{F_{\mathrm{r}}} - \sin\mathscr{D}\cos\mathscr{I})/\sin\mathscr{I}\,, \tag{12}$$

$$Q_{\mathrm{q}} = Q_{F_{\mathrm{q}}}/\sin\mathscr{I} \tag{13}$$

(Hitchman 1999), where $\mathscr{D}$ is the local declination angle. Again, for Australian stations, $\mathscr{D}$ may be taken from Lewis & McEwin (1996).

3 EXPERIMENTS

Observations from three different experiments are analysed in this paper. Fig. 1 shows the sites from which the data have originated.

The techniques are first demonstrated in Section 4 with aeromagnetic base-station data from the Murray Basin region of Australia. In this instance the corresponding reference variations were recorded in the geographic frame at the Canberra Magnetic Observatory (CNB).

Section 5 then presents an analysis of data recorded by a floating magnetometer anchored at three different sites in succession on the continental shelf. The instrument was deployed during the Southern Waters of Australia Geoelectric and Geomagnetic Induction Experiment (SWAGGIE) (see White *et al.* 1998), and the data observed are used to test the techniques for floating total-field instruments. Horizontal reference data are taken from a land site, One Tree Hill (OTH). There are three such 'Anchor-mag' data sets.

Section 6 presents an analysis of data recorded by a magnetometer released to drift freely over deep ocean. This instrument was also deployed during the SWAGGIE experiment. There are two such 'Floater-mag' data sets, each of some four days duration. Reference horizontal variations for these Floater-mag data were taken from CNB, and from sites on land (OTH) and seafloor (Twosome, TW) that were part of the SWAGGIE experiment.

The magnetic data analysed in this paper have thus been observed by a variety of instruments, the specifications of which are listed in Table 2. The OTH and TW magnetometers are of Flinders University development and construction, and are based on the design described by Chamalaun & Walker

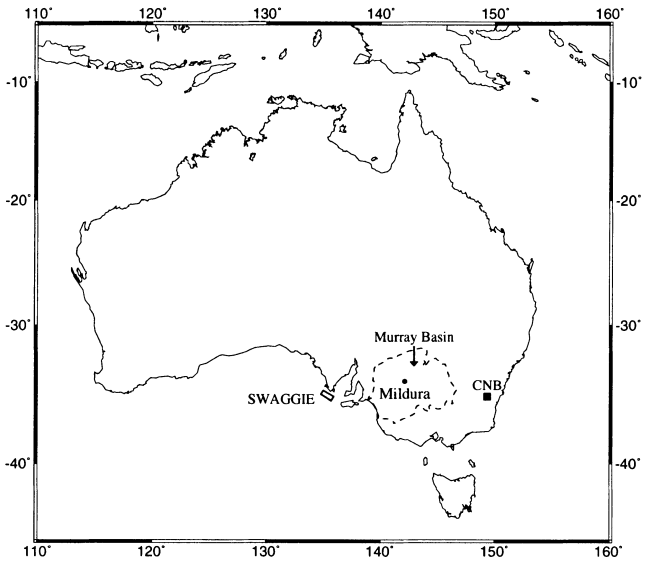

Figure 1. Map of Australia showing the sites referred to in the present paper.

Table 2. Magnetometers used in the present study for recording time variations of the magnetic field.

Station	Magnetometer type	Sample interval (s)
CNB	Three-component fluxgate	1
OTH	Three-component fluxgate	10
TW	Three-component fluxgate	60
Mildura	Total-field proton precession	5
Anchor-mag	Total-field proton precession	10
Floater-mag	Total-field Overhauser	3

(1982). The TW magnetometer is one of an array packaged for seafloor deployment, and continues the tradition of White (1979) and White *et al.* (1990).

These present fluxgate instruments incorporate a number of recent modifications and developments. They use ring-core fluxgate sensors, and record data on solid-state memory.

4 OBSERVED DATA

The total-field data are generally recorded in time-series that can be taken directly as nanotesla, and used accordingly. The magnetic field variations recorded by fluxgate instruments have first been scaled using the appropriate calibration values, determined experimentally at Flinders University. Data from the seafloor instrument (TW) have been corrected for any tilt of the instrument on the seafloor, using tilt data monitored mechanically by the instrument and recorded internally with the magnetic data. The time-series for the magnetic sensors of both OTH and TW are then mathematically rotated for alignment with magnetic north to give $h(t)$ and $d(t)$ time-series.

Certain basic editing, mainly for data spikes, has been carried out in places. The data most in need of editing were those from the Anchor-mag deployments, although this is not thought to result from that particular style of deployment. The

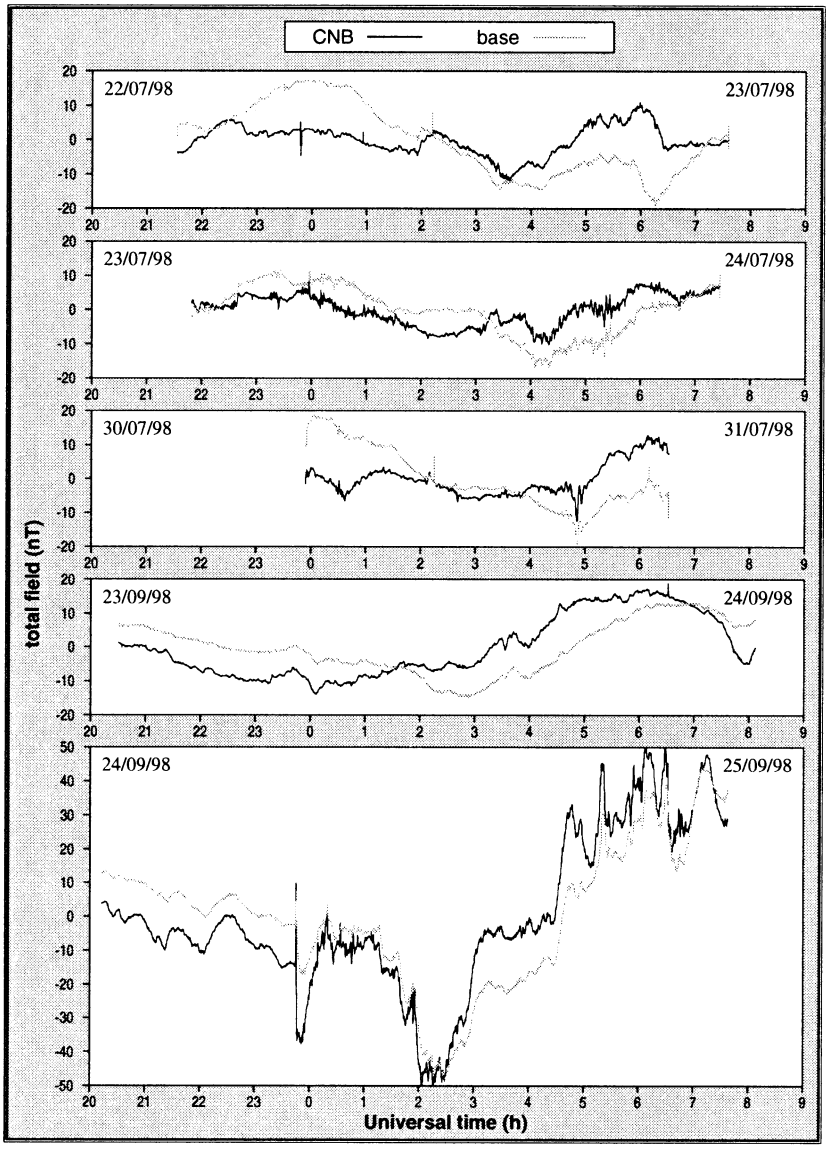

Figure 2. Examples of simultaneous data from the aeromagnetic base stations Mildura A (upper three panels) and Mildura B (lower two panels), and Canberra Magnetic Observatory (CNB). The base-station data were observed as $f(t)$ time-series, while the CNB signals have been computed from observed traditional components, $x(t)$, $y(t)$ and $z(t)$. All $f(t)$ traces are plotted relative to arbitrary baselines.

Anchor-mag data contain many false readings, all clearly underestimating the strength of Earth's magnetic field. Such behaviour is common in proton-precession magnetometers that are not operating optimally. In the present case the data have been filtered by replacing each data point with the third highest reading from the set of 21 consecutive readings (at 10 s intervals) centred on that point. The spacing of independent points is 210 s after this process and results given for the Anchor-mag data are, therefore, restricted to periods of 420 s and longer.

Further beneficial treatment for noise spikes and other errors occurs in the analysis of the basic magnetometer time-series. For example, the transfer functions that determine the induction arrows are computed using the RRRMT routine of Chave *et al.* (1987), which employs robust statistics to downweight outliers arising from erroneous instrument performance.

Similarly, transfer function determination using data from a land reference station such as OTH helps suppress signals in the records of a floating magnetometer that are due to the motional induction of ocean swell (Weaver 1965). The ocean swell signal may be so strong over a limited bandwidth, however, that the determination of arrows in that bandwidth is best avoided, as shown in one of the examples below.

Numerical values for the transfer functions supporting the induction arrows presented in this paper are tabulated in Hitchman (1999).

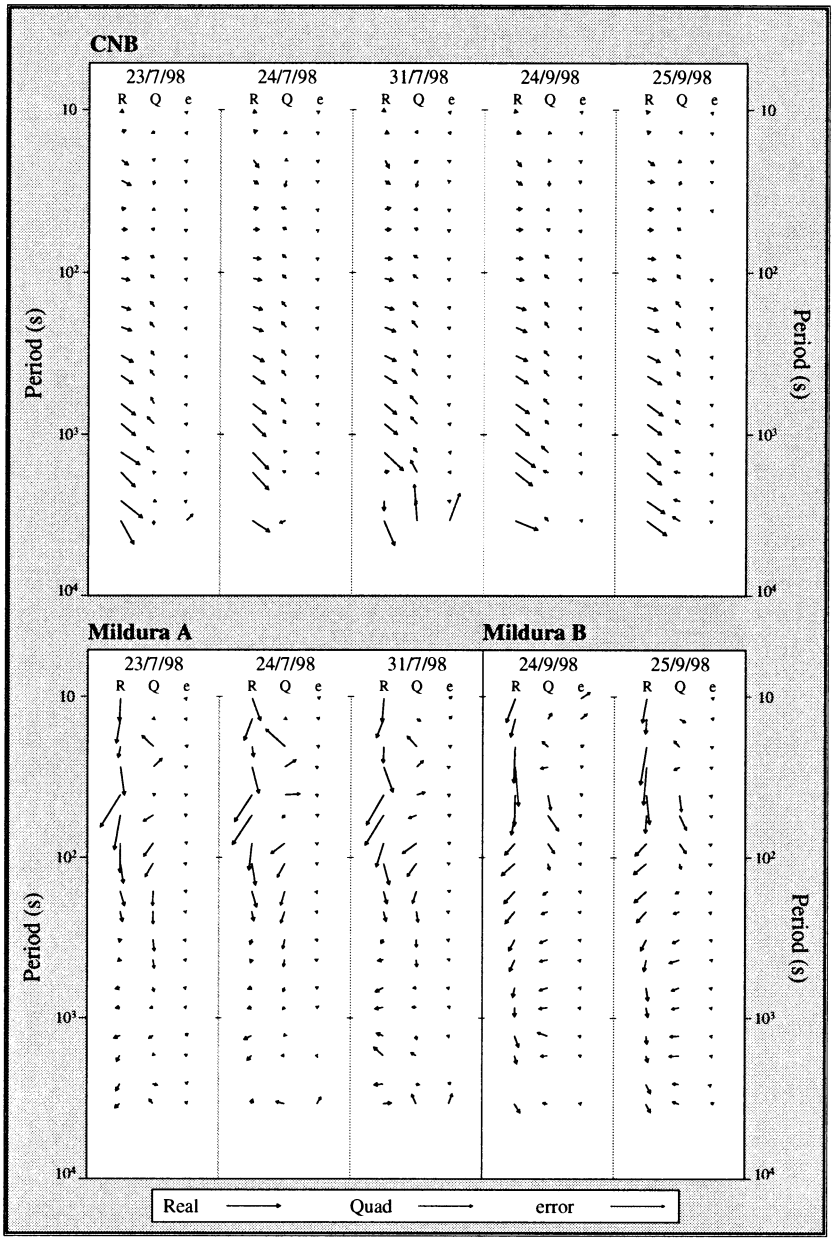

Figure 3. Real and quadrature induction arrows determined for CNB and for stations Mildura A and Mildura B. Geographic north is to the top of the diagram. The period range shown is 10–3500 s. All arrows have been determined from total-field signals for the relevant site, combined with horizontal fluctuation records, $x(t)$ and $y(t)$, from CNB. In the columns, R, Q and e denote real, quad and error, respectively. The arrows at the bottom of the figure are each of unit length, for scale.

5 AEROMAGNETIC BASE-STATION DATA IN WESTERN VICTORIA

Data have been procured for two sites in the Mildura region, here called Mildura A and Mildura B, at which time-series of the total field were recorded by an instrument run as a base-station monitor for aeromagnetic surveys. The exact positions of Mildura A and Mildura B are undeclared, consistent with the proprietary nature of the survey data. However, knowledge that the general location is the Murray Basin, in the vicinity of Mildura, is sufficient for present purposes.

The Canberra Magnetic Observatory (CNB) has been taken as a reference station for the Mildura total-field data. Originally recorded at 1 s intervals, the CNB data have been resampled at 5 s intervals to be consistent with the Mildura records. Following this resampling, the CNB $x(t)$, $y(t)$ and $z(t)$ data have first been used to construct an $f(t)$ series for CNB, for comparison. Examples of simultaneous field fluctuations are shown in Fig. 2.

The horizontal data, $x(t)$ and $y(t)$ for CNB, were then used to determine transfer functions and induction arrows for the two Mildura sites using eqs (9)–(13). The data have been analysed on a day-by-day basis. As a control, transfer functions were determined for CNB using the same horizontal field data and the CNB reconstructed $f(t)$ series. The results for both the Mildura and Canberra arrows are presented in Fig. 3.

In Fig. 3, for a given site and a given day, there are three columns of arrows. The left column with heading R shows real arrows, the centre column with heading Q shows quad arrows, and the third column with heading e shows error arrows. It is the amplitude of the error arrows that is important, rather than their orientation.

The first remark to make, upon inspection of Fig. 3, is that the method of using total-field variations to give transfer functions and induction arrows appears to have worked well. There is pleasing consistency, not only across the five determinations for the 'control', CNB, but also across the three determinations for Mildura A and the two determinations for Mildura B. The errors, in almost all cases, are small. The CNB arrows agree with previous determinations for Canberra (see e.g. Ferguson 1988; Milligan 1988; Kellett *et al.* 1991). The Mildura arrows are reasonable in terms of previous, longer-period arrow determinations for the area (Lilley & Bennett 1972).

The distinctive patterns as period changes for both Mildura A and B appear to be well determined. The characteristics of

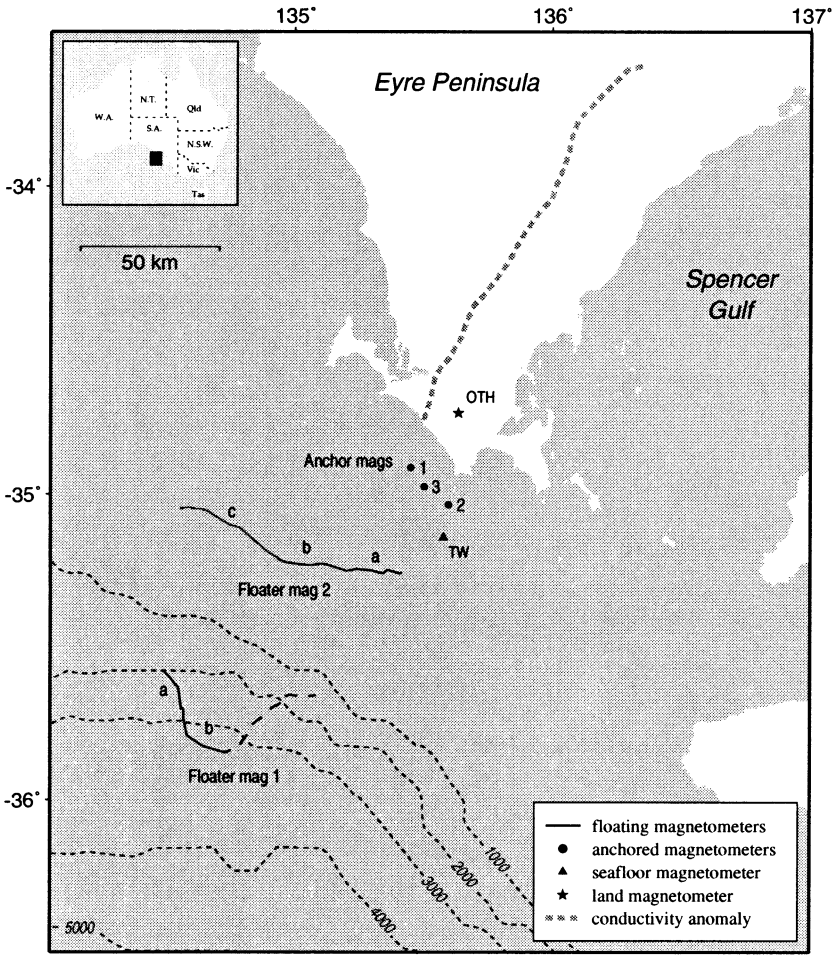

Figure 4. The region of the SWAGGIE experiment, South Australia, and the location of the Eyre Peninsula conductivity anomaly on land (Kusi 1996). The sites of the three 'Anchor-mag' deployments are shown, with, further out to sea, the tracks taken by the drifting 'Floater-mags'. Also shown are the positions of the reference stations OTH (on land) and TW (seafloor).

the arrow patterns in Fig. 3 are sufficiently different to indicate that the data are from two distinctly different sites. Differences in the arrow patterns for Mildura A and B, particularly in the period range 50–200 s, are taken to indicate different local conductivity structure.

6 FLOATING MAGNETOMETERS ANCHORED OFF THE EYRE PENINSULA, SOUTH AUSTRALIA

The method is now applied to data from a total-field magnetometer that floated at the sea surface whilst tethered to the seafloor. Part of the SWAGGIE exercise, this instrument was anchored for durations of several days at three sites in succession over the continental shelf of South Australia. The positions of these three sites are shown in Fig. 4. Water depth at the sites where the floating magnetometer was anchored is typically 90 m, and the sites, Anchor-mag 1, 2 and 3, are typically 5 km from the coast.

The sites were chosen to span a possible offshore position of the 'Eyre Peninsula Conductivity Anomaly' (EPA) (White & Milligan 1984; Milligan 1989). This conductivity structure has a strong effect on the natural fluctuating magnetic field on land. Onshore it has been mapped in detail right up to the coastline, which it intersects approximately at right-angles (Kusi *et al.* 1998).

For the Anchor-mag data, the onshore site OTH has been taken as a reference station. At OTH a three-component fluxgate instrument recorded every 10 s. Reconstructed $f(t)$ signals for OTH are presented with simultaneous Anchor-mag records in Fig. 5. Horizontal data from OTH were used in combination with the Anchor-mag data to produce transfer functions and arrows for the Anchor-mag sites using eqs (3)–(7). Where sufficiently long time-series are available such as at Anchor-mag 1 and 3 the data have been divided into segments, and independent determinations of transfer functions made. In this way, induction arrows have been checked for consistency at these sites. The data segments used for separate determinations of transfer functions at Anchor-mag 1 and 3 are marked as 'a' and 'b' in Fig. 6. The beginning and endpoints of these segments have been selected so that the trend over the segment is zero.

Arrows from the three Anchor-mag sites are presented in Fig. 6. The top panel of the figure shows the arrows determined using segments a and b at sites 1 and 3. The arrows in the bottom panel have been obtained using data from the

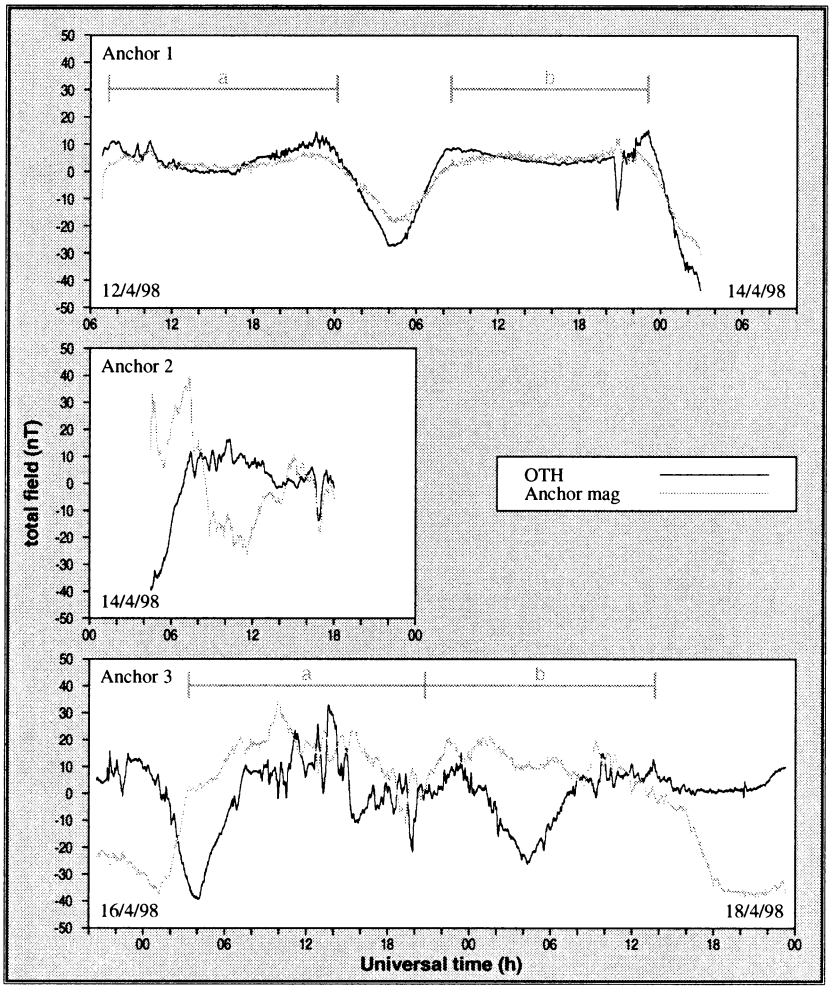

Figure 5. Examples of simultaneous data from the Anchor-mag stations and OTH. The Anchor-mag data are observed total-field $f(t)$, while the OTH $f(t)$ signals have been reconstructed from observed components $h(t)$, $d(t)$ and $z(t)$. All $f(t)$ traces are plotted relative to arbitrary baselines. The segments of the Anchor-mag 1 and 3 time-series marked a and b have been used for induction arrow determination.

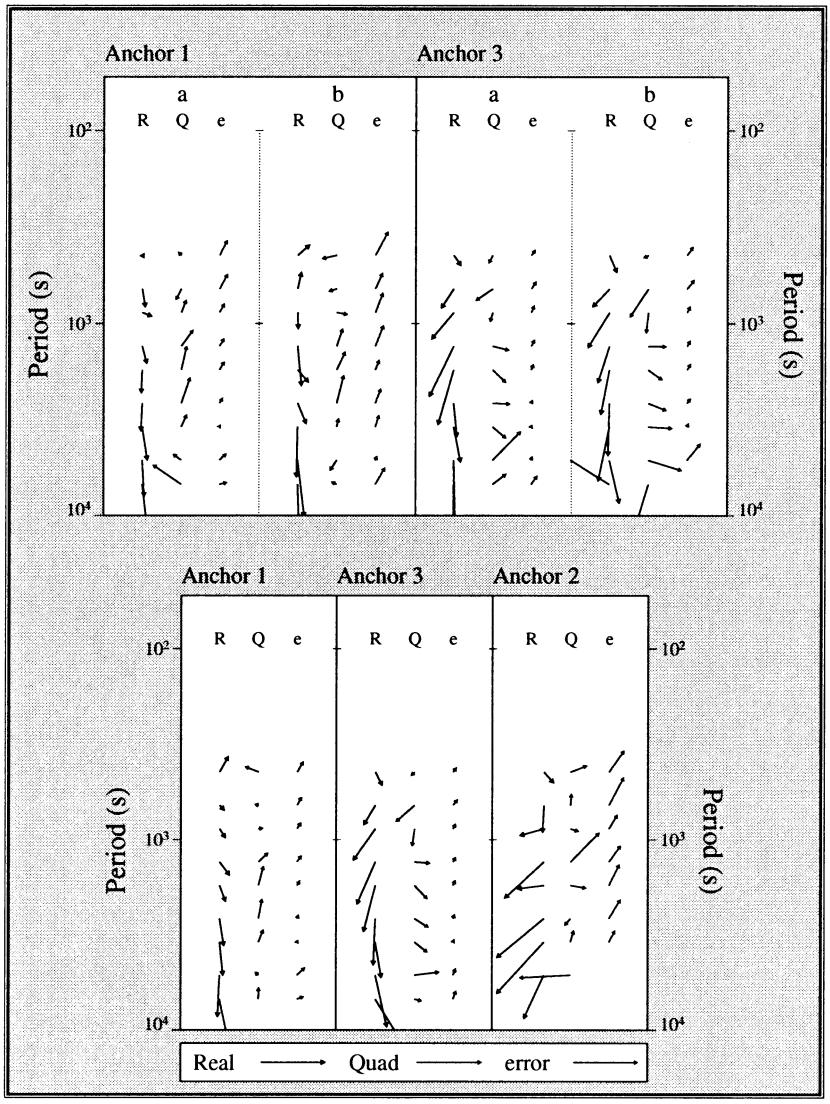

Figure 6. Real and quadrature induction arrows determined for the the Anchor-mag sites 1, 2 and 3. Geographic North is to the top of the figure. All arrows have been determined from total-field records at the relevant site, combined with horizontal fluctuation records, $h(t)$ and $d(t)$, from OTH. In the top panel, arrows for sites 1 and 3 have been derived from independent segments of the time-series, identified in Fig. 5. In the bottom panel, columns are in order of increasing easterly longitude from left to right across the figure. The format of arrow presentation and errors is as for Fig. 3.

beginning of segment a to the end of segment b at sites 1 and 3, and all the data from site 2. A first inspection of this figure gives confidence that the method applied to total-field data from a floating magnetometer has given good results. The arrow patterns are generally consistent between data segments at sites 1 and 3. When the full time-series have been used (Fig. 6, bottom panel), errors are small, except where there is obvious 'noise' in the arrow patterns. Errors tend to increase for arrows determined using segments of the time-series at sites 1 and 3 (Fig. 6, top panel). The general southward orientation of the arrows at all three Anchor-mag sites is consistent with the 'coast effect' caused by the body of seawater in the Great Australian Bight and Southern Ocean. In fact, while the coast effect of South Australia has been observed by seafloor instruments (White & Heinson 1994), the present results are the first observations (perhaps anywhere?) of the coast effect at the sea surface.

Reference to Fig. 4, then, strongly suggests the Eyre Peninsula conductivity anomaly continues offshore and passes between Anchor-mag sites 1 and 3. Such a strike for the EPA is consistent with the aeromagnetic pattern for the area. That a conductivity anomaly can thus be detected below and in the presence of a sheet of ocean water some 100 m thick is an important aspect of marine electromagnetic studies to have demonstrated.

7 MAGNETOMETERS FLOATING FREE IN THE DEEP OPEN OCEAN, GREAT AUSTRALIAN BIGHT

As a further trial of this technique, it has been applied to data from a free-floating magnetometer. This instrument was deployed during SWAGGIE, and its position monitored by satellite

navigation. In this case the instrument was an Overhauser magnetometer (see Table 2), set to record at intervals of 3 s. Two deployments of some four days each were achieved, and the paths along which the magnetometer drifted during these times are shown in Figs 4 and 7.

The free-floating magnetometer drifted at speeds typically of the order of 0.5 knot (approximately 0.3 m s^{-1}). Magnetic pulsations and substorm fluctuations are thus recorded against the signal of the magnetometer moving across the crustal magnetization patterns of the seafloor. However, the latter appear in the data as slow variations with time and, upon spectral analysis, do not contribute to the part of the spectrum of main interest. A further major filtering of such effects is provided by the procedures followed when employing the reference station data to determine transfer functions. The reference stations used were stationary, so contain none of the 'changing crustal magnetization' signal of the Floater-mag data.

As shown in Fig. 4, the Floater-mag data have been further divided into sectors a and b for Floater-mag 1 and a, b and c for Floater-mag 2 to test if such sectors are individually viable for arrow determination. Simultaneous data from the various Floater-mag sectors and the reference stations used for them are shown in Fig. 8.

Due to the logistic arrangements of the SWAGGIE deployments, Floater-mag 1 was recording before OTH was operational. Thus, Floater-mag 1a uses CNB as a reference for horizontal-field data, Floater-mag 1b uses the seafloor instrument TW as soon as the TW recording period commences, and Floater-mag 2a, b and c use OTH as soon as OTH starts its recording period. These reference magnetometers CNB, TW and OTH, being stationary, will contain no changing crustal magnetization signal, and so provide no coherence support of such signals in transfer function determinations. Similarly, while the Floater-mag data, observing every 3 s, contain swell-generated magnetic signals at periods typically of 13 s (which will be the subject of a separate analysis), again using land reference data for the determination of their transfer function and induction-arrow values guards against contamination of these results by the motional induction signal of ocean swell.

Arrows from the various Floater-mag sectors are presented in Fig. 9. While the Anchor-mag data represented the step from land (such as the Murray Basin sites) to a magnetometer floating on the sea surface, the present Floater-mag data represent a further step to a floating magnetometer that drifts freely with the ocean currents. Thus, the Floater-mag data have a component of geological signal, evident in Fig. 8. Similarly, the conductivity structure traversed by a floating magnetometer may not be uniform. In cases of uniform structure, the transfer functions might reasonably be expected to reflect local structure well. However, when traversed structure is non-uniform, transfer functions are an 'average' response to the geology. The exact nature of such an average is difficult to quantify as it depends significantly on the path and speed of the drifting magnetometer and on the conductivity structure. This averaging process will tend to degrade the transfer function response to conductivity structure, and may disguise subtle responses.

It is, however, pleasing to see in Fig. 9 that again the methods for determining transfer functions and induction arrows seem to have worked satisfactorily. While the differences between the Floater-mag 1a and 1b patterns may be real, as the areas over which they have sampled are tens of kilometres apart, these differences may also be due at least in part to the different

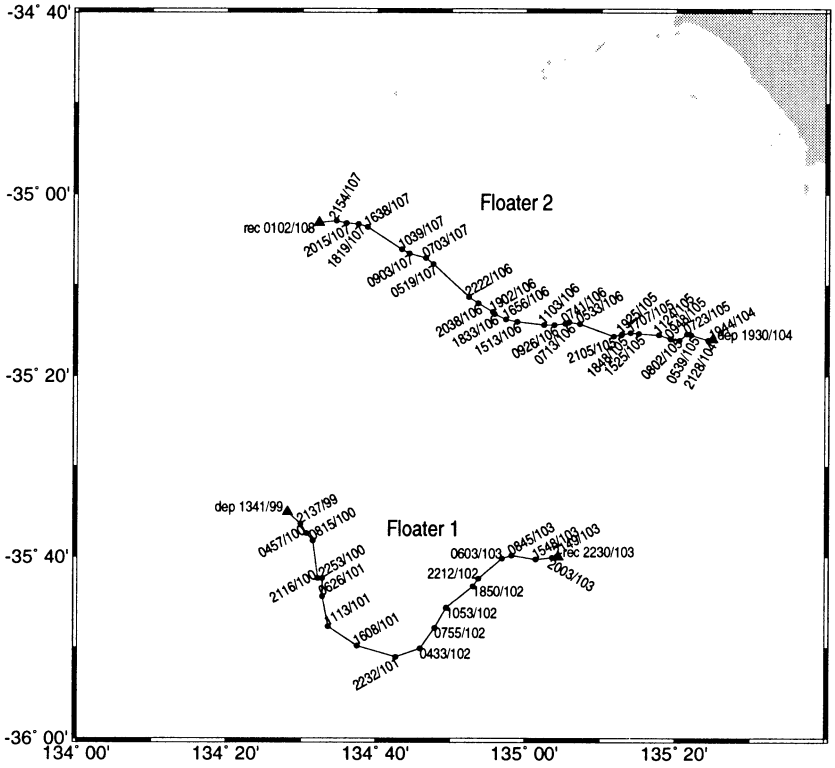

Figure 7. The paths recovered from satellite navigation data traversed by the Floater-mag 1 and Floater-mag 2 magnetometer deployments in April 1998 during the SWAGGIE deployment cruise. The position data are in the format UT time/day number.

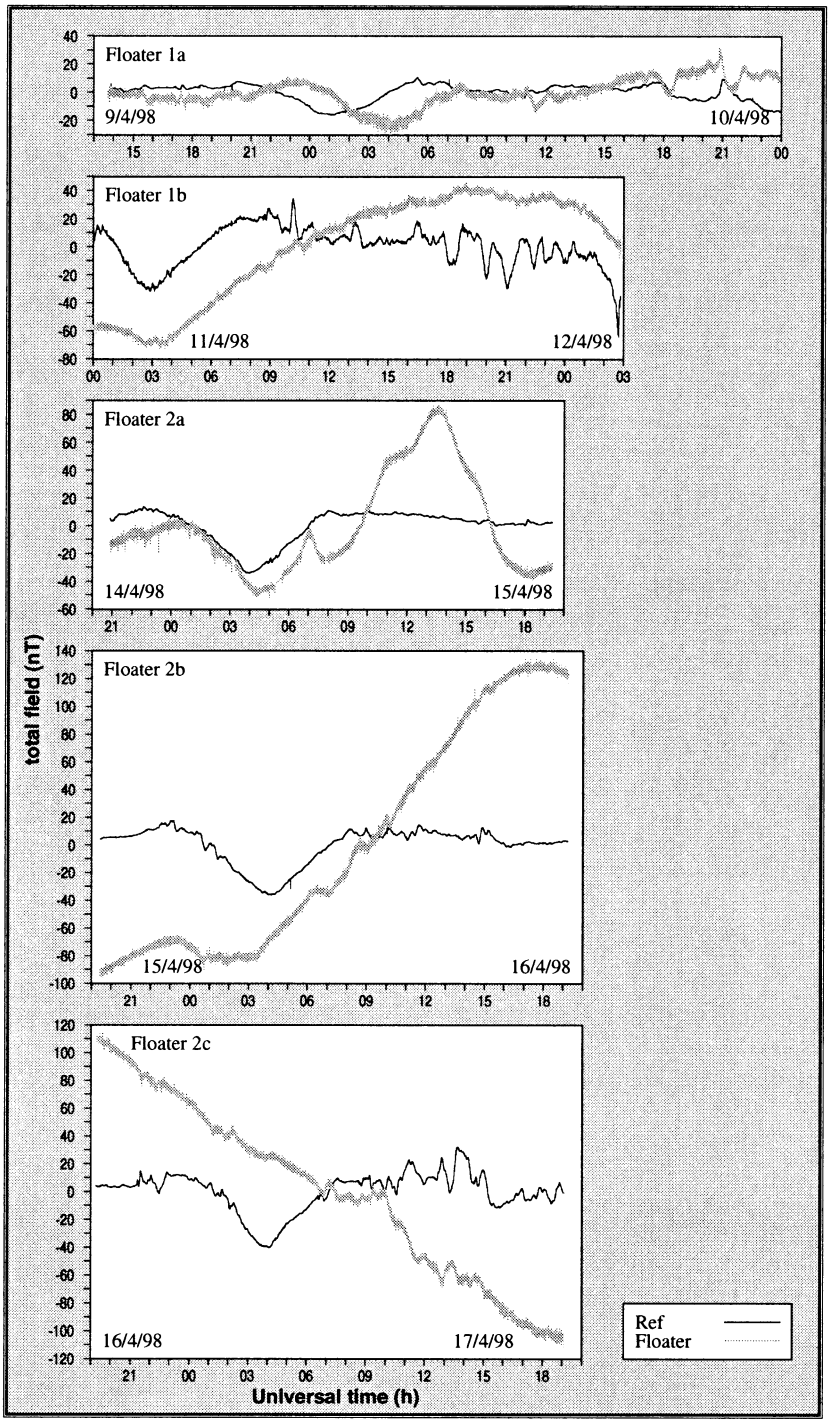

Figure 8. Examples of simultaneous data from the Floater-mag data sets and various reference stations, as explained in the text. The Floater-mag data are observed total-field $f(t)$, while the reference $f(t)$ signals have been calculated from observed traditional components, $x(t)$, $y(t)$, $z(t)$, or $h(t)$, $d(t)$, $z(t)$. All $f(t)$ traces are relative to arbitrary baselines. The thick trace of the Floater-mag data is attributed to the presence of a magnetic signal generated by ocean swell.

reference stations used (CNB and TW). However, for Floater-mag 2a, 2b and 2c, a single reference station was used (OTH); when errors are taken into account, these arrow patterns are pleasingly consistent.

Regarding arrow direction, generally Floater-mag arrows have a consistent southward orientation. This characteristic suggests that variations at Floater-mag sites are primarily influenced by the coast effect. There is no clear evidence from the arrow patterns to suggest that the Floater-mag variations have been influenced by the EPA.

While the deep water may have masked detection of the EPA by the Floater-mag data, Fig. 9 suggests that the EPA path

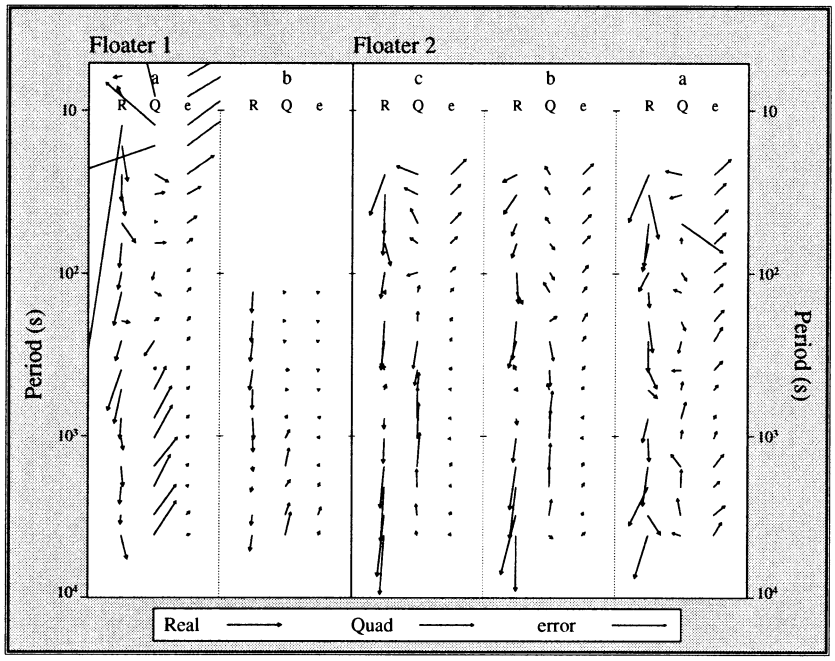

Figure 9. Real and quadrature induction arrows determined for the Floater-mag data sets. Geographic north is to the top of the diagram. All arrows have been determined from total-field records from the Floater-mag, combined with horizontal fluctuation records, $h(t)$ and $d(t)$, from the variety of sources explained in the text. From left to right across the figure, the columns are in order of increasing easterly longitude. The format of arrow presentation and errors is as for Fig. 3.

may cross the continental shelf to the east of the Floater-mag paths. Also, it is possible that the EPA is a feature of the continental crust that is present on the continental shelf, and may terminate at the continental slope. The EPA may well not continue across the deep ocean floor, which has a very different geological structure and history.

8 CONCLUSIONS

The conclusion reached is that useful transfer-function estimates have been obtained from the total-field magnetometer observations. As many magnetic survey parties operate 'storm warning' recording total-field magnetometers, it is demonstrated that all of them are possible GDS sites in the reconnaissance of a large continent such as Australia. Reference horizontal data are needed, and where a network of magnetic observatories spans a continent, such observatory data may have application over horizontal distances of hundreds of kilometres.

Similarly, floating magnetometers at sea are possible GDS sites, both anchored and floating free. These techniques may be useful where seafloor magnetometers are not available or for some reason are impractical. Where seafloor magnetometers are in use, surface total-field magnetometers may usefully supplement their observations.

It is left to an analysis of the full SWAGGIE data set to discuss evidence for the Eyre Peninsula Conductivity Anomaly offshore. However, the results of this paper suggest that the EPA is apparent in surface total-field data from Anchor-mag sites near the coast but not in Floater-mag data from deeper water beyond the edge of the continental shelf, possibly offset from the strike of the EPA.

ACKNOWLEDGMENTS

We acknowledge the assistance given to this research by Steve Mudge, now of Vector Research Pty Ltd, and Grant Donnes, UTS Geophysics, in providing the Mildura region aeromagnetic base-station data, and by the AGSO Geomagnetism section in providing the Canberra Magnetic Observatory data. Antony White and Graham Heinson, our collaborators in SWAGGIE, have assisted in many ways. The skill of the captain and crew of the Research Vessel *Franklin* made possible the exercises with the anchored and floating-free magnetometers. Hiroake Toh helped with the deployment and retrieval of the instruments, and Steven Constable provided advice and mooring equipment. We have benefited from discussion of this project with many people, especially Charles Barton, Paula Hahesy, Dudley Parkinson and Jonathon Whellams. We are grateful to Susan Macmillan and Malcolm Ingham for comments that have significantly enhanced this paper. APH acknowledges the support of an Australian National University Research Scholarship. PRM publishes with the permission of the Executive Director, AGSO.

REFERENCES

Blakely, R.J., 1995. *Potential Theory in Gravity and Magnetic Applications,* Cambridge University Press, Cambridge.

Chamalaun, F.H. & Walker, R., 1982. A microprocessor based digital fluxgate magnetometer for geomagnetic deep sounding studies, *J. Geomagn. Geoelectr.,* **34,** 491–507.

Chave, A.D., Thomson, D.J. & Ander, M.E., 1987. On the robust estimation of power spectra, coherences and transfer functions, *J. geophys. Res.,* **92,** 633–648.

Ferguson, I.J., 1988. The Tasman project of seafloor magnetotelluric exploration, *PhD thesis,* the Australian National University, Canberra.

Filloux, J.H., 1987. Instrumentation and experimental methods for oceanic studies, in *Geomagnetism,* Vol. 1, pp. 143–247, ed. Jacobs, J.A., Academic Press, London.

Gough, D.I., 1989. Magnetometer array studies, earth structure, and tectonic processes, *Rev. Geophys.,* **27,** 141–157.

Gough, D.I. & Ingham, M.R., 1983. Interpretation methods for magnetometer arrays, *Rev. Geophys. Space Phys.,* **21,** 805–827.

Heinson, G., Constable, S. & White, A., 1996. Seafloor magnetotelluric sounding above Axial Seamount, *Geophys. Res. Lett.,* **23,** 2275–2278.

Hitchman, A.P., 1999. Interactions between aeromagnetic data and electromagnetic induction in the Earth, *PhD thesis,* the Australian National University, Canberra.

Hobbs, B.A., 1992. Terminology and symbols for use in studies of electromagnetic induction in the earth, *Surv. Geophys.,* **13,** 489–515.

Kellett, R.L., Lilley, F.E.M. & White, A., 1991. A two-dimensional interpretation of the geomagnetic coast effect of southwest Australia, observed on land and seafloor, *Tectonophysics,* **192,** 367–382.

Kusi, R., 1996. Electromagnetic induction studies in the Eyre Peninsula, South Australia, *PhD thesis,* the Flinders University of South Australia.

Kusi, R., White, A., Heinson, G. & Milligan, P., 1998. Electromagnetic induction studies in the Eyre Peninsula, South Australia, *Geophys. J. Int.,* **132,** 687–700.

Lewis, A.M. & McEwin, A.J., 1996. *The Geomagnetic Field in the Australian Region, Epoch 1995.0,* Aust. Geol. Surv. Org.

Lilley, F.E.M., 1991. Electrical conductivity anomalies in the Australian lithosphere: effects on magnetic gradiometer surveys, *Expl. Geophys.,* **22,** 243–246.

Lilley, F.E.M. & Arora, B.R., 1982. The sign convention for quadrature Parkinson arrows in geomagnetic induction studies, *Rev. Geophys. Space Phys.,* **20,** 513–518.

Lilley, F.E.M. & Bennett, D.J., 1972. An array experiment with magnetic variometers near the coasts of southeast Australia, *Geophys. J. R. astr. Soc.,* **29,** 49–64.

Lilley, F.E.M., Sloane, M.N. & Ferguson, I.J., 1984. An application of total-field magnetic fluctuation data to geomagnetic induction studies, *J. Geomag. Geoelectr.,* **36,** 161–172.

Milligan, P.R., 1988. Short-period transfer-function vectors for Canberra and Charters Towers magnetic observatories, *J. Geomagn. Geoelectr.,* **40,** 95–103.

Milligan, P.R., 1989. Geomagnetic variations in Southern Australia: the Eyre Peninsula anomaly, *PhD thesis,* the Flinders University of South Australia.

Palshin, N.A., 1996. Oceanic electromagnetic studies: a review, *Surv. Geophys.,* **17,** 455–491.

Parkinson, W.D., 1983. *Introduction to Geomagnetism,* Scottish Academic Press, Edinburgh.

Parkinson, W.D. & Hutton, V.R.S., 1989. The electrical conductivity of the earth, in *Geomagnetism,* Vol. 3, pp. 261–321, ed. Jacobs, J.A., Academic Press, London.

Weaver, J.T., 1965. Magnetic variations associated with ocean waves and swell, *J. geophys. Res.,* **70,** 1921–1929.

Weaver, J.T., 1994. *Mathematical Methods for GeoElectromagnetic Induction,* Research Studies Press, Taunton.

White, A., 1979. A seafloor magnetometer for the continental shelf, *Mar. geophys. Res.,* **4,** 105–114.

White, A. & Heinson, G., 1994. Two-dimensional electrical conductivity structure across the southern coastline of Australia, *J. Geomag. Geoelectr.,* **46,** 1067–1081.

White, A. & Milligan, P.R., 1984. A crustal conductor on Eyre Peninsula, South Australia, *Nature,* **310,** 219–222.

White, A., Kellett, R.L. & Lilley, F.E.M., 1990. The continental slope experiment along the Tasman Project profile, southeast Australia, *Phys. Earth planet. Inter.,* **60,** 147–154.

White, A., Heinson, G., Constable, S., Milligan, P., Lilley, F.E.M. & Toh, H., 1998. Magnetotelluric exploration of the Eyre Peninsula electrical conductivity anomaly, *Preview,* **76,** 91–92.